Exploring metal nanoparticles for matter-wave interferometry

Sebastian Pedalino, Tomás de Sousa, Yaakov Y. Fein, Stefan Gerlich, and Markus Arndt[*,†]

University of Vienna, Faculty of Physics, Quantum Nanophysics, VCQ, Boltzmanngasse 5, A-1090 Vienna, Austria
and University of Vienna, Vienna Doctoral School in Physics, Boltzmanngasse 5, A-1090 Austria

High-mass matter-wave interferometry opens interesting perspectives for testing fundamental physics while posing intriguing challenges in experimental technologies. Here we explore the source and detection techniques that will be the basis for the next generation of quantum experiments with objects at least one order of magnitude more massive than the current state of the art. Magnetron sputtering provides a means to produce a continuous metal cluster beam with a large variability in material composition, structure, temperature, velocity, electric, and magnetic properties. The mass-scalable nanoparticles come with high ionization yield and a detected beam brilliance of up to 10^{11} sr^{-1} s^{-1} clusters. We find favorably slow and narrow velocity distributions for mass-filtered clusters up to 800 kDa, which can also be readily ionized, manipulated, and detected by 266 nm UV laser light. The source-detector combination that we demonstrate here fulfills the essential requirements for a next generation of nanoparticle interferometry.

I. INTRODUCTION

Matter-wave interferometry with massive objects is attracting a growing interest as a paradigmatic example of quantum physics at the interface to classical phenomena. Many speculations have emerged on how matter-wave research could contribute to testing spontaneous [1] or gravitationally induced wave function collapse [2,3], probe nonstandard decoherence, potentially by light dark matter [4], or mesoscopic remnants of microscopic space-time fluctuations [5]. At very high masses it could probe dephasing caused by the gravitational redshift [6] and one might probe the universality of free fall with quantum particles across a mass range and material diversity that cannot be covered by any other present experiment [7]. On top of such fundamental considerations, it is an important task to explore how far we can push experimental tests of the quantum superposition principle, since its transition to classical observations is still at the heart of ongoing debates on the foundations of physics. Recent experimental demonstrations of very massive or widely delocalized quantum systems include cryogenic cantilevers [8] or trapped nanoparticles in their ground states [9] as well as matter-wave interference of neutrons [10] or atoms [11] in superpositions extending over 10–50 cm. Even families of tailored, hot molecules beyond 25 kDa [12] and antibiotic polypeptides [13] have been seen to reveal their matter-wave

nature. Our present work prepares a different line of research targeting high-mass interferometry with metal clusters well beyond 10^5 Da.

Several particle sources have already been explored in the past: Direct nanosecond laser desorption (ns-LD) from a moving powder plate has proven useful in launching intact families of tailored organic molecules [14] as well as atomically defined metallic giant nanoparticles [15]. Pulsed laser desorption was also key in demonstrating matter-wave interference with tailored macromolecules [12]. Such sources usually generate beams of internally hot particles with limited brilliance and broad velocity distributions (100–200 m/s) even for particles in the 10–100 kDa range. Similar or higher velocities are observed in the neutral part of the plume ejected by matrix-assisted laser desorption ionization (MALDI) [16,17]. In contrast to these direct laser desorption methods, laser-induced acoustic desorption can launch neutral 10 kDa molecules as slow as 20 m/s [18] and silicon nanospheres of 10 GDa even below 1 m/s [19]. Laser-induced acoustic desorption has also proven valuable for loading electrical traps in mass spectrometry [20] and quantum optics [21] but generally produces dilute and divergent beams.

In our present work we focus on a different material class for matter-wave interferometry, specifically metal nanoparticles and explore a suitable particle source, its velocity distribution and the ionization efficiency with regard to the requirements of our next-generation matter-wave interferometer [22]. In matter-wave experiments, the time for the wave function to expand increases with the particle mass. A Talbot-Lau interferometer with 133 nm period gratings will require particles slower than 150 m/s for masses beyond $m = 150$ kDa, as indicated by Fig. 5. We find magnetron sputtering to be a promising source and we identify continuous deep UV ionization as a useful detection technique. Both are scalable in mass and material composition.

*markus.arndt@univie.ac.at
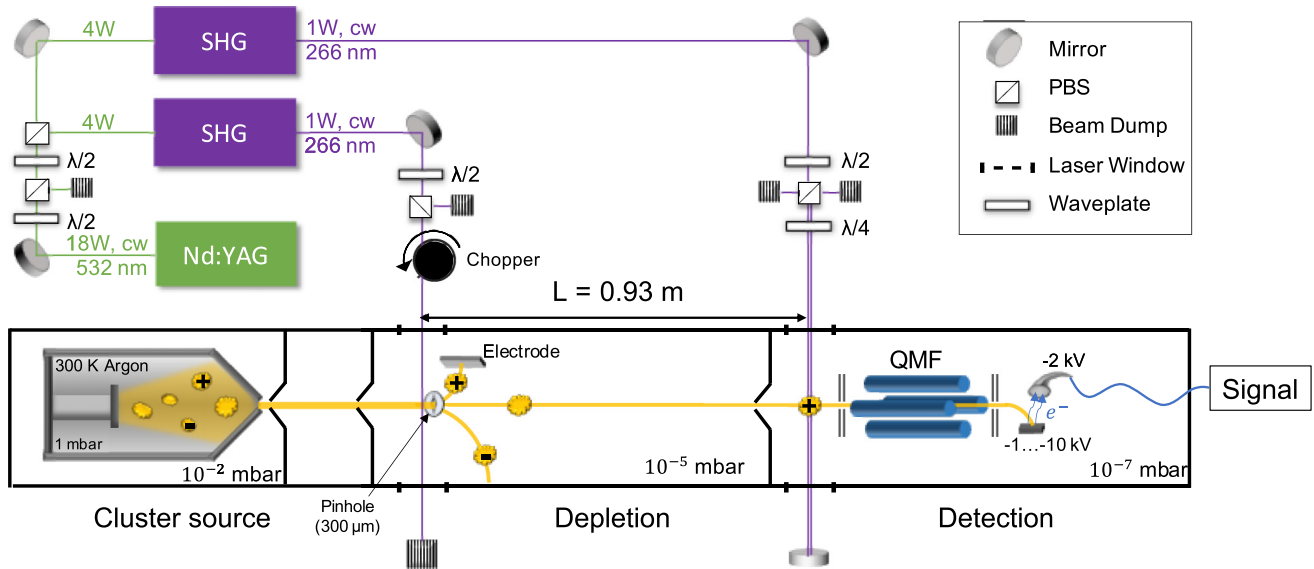†http://www.quantumnano.at

FIG. 1. A DC magnetron sputters a metal target in pure argon. Cluster aggregation occurs at 300 K at a base pressure of 1 mbar. The gas flow carries singly charged and neutral clusters through a 1–5 mm variable iris first into a chamber at about 0.01 mbar, then through differential pumping stages into a quadrupole mass filter at 1×10^{-7} mbar. A first interaction zone allows UV-ionization beam depletion of the neutral cluster beam. The first UV laser along the molecular beam path is used to measure the relative depletion efficiency as well as the velocity distribution and the absolute photoionization cross sections of the clusters. A second UV interaction zone at the entrance of the quadrupole mass filter is used to compare photoionization with electron impact efficiency. Ions up to 3 MDa can be filtered with $\Delta m/m \geqslant 5\%$ and be detected by an electron multiplying detector after impact on a conversion dynode.

Possible ways to realize matter wave-front division (beam splitting) in depletion gratings can be for example via fragmentation [23] or photocleavage [24]. Here we study the efficiency of photoionization [25,26], with continuous rather than with pulsed gratings. We make use of the photoelectric effect and chose metals with work functions significantly below the energy of a single photon at 4.6 eV.

II. EXPERIMENT

Magnetron sputtering is a widely used method in cluster beam science [27]. We use a water-cooled DC magnetron (Oxford Applied Research) with an argon plasma at an electrical power of up to 150 W. For masses up to 250 and 600 kDa we explore yttrium and hafnium. Both materials feature a low bulk work function of $W(\mathrm{Y}) = 3.1$ eV and $W(\mathrm{Hf}) = 3.9$ eV, enabling photoionization under continuous (cw) deep-UV (266 nm, 4.6 eV) laser irradiation. They also exhibit small magnetic susceptibilities which avoids magnetic dephasing in quantum experiments: $\chi(\mathrm{Y}) = 12 \times 10^{-4}$ m^3/mol and $\chi(\mathrm{Hf}) = 7.0 \times 10^{-5}$ m^3/mol. Their high melting points $[T_m(\mathrm{Y}) = 1799$ K and $T_m(\mathrm{Hf}) = 2506$ K] favors the generation of larger seed particulates and larger clusters. Since yttrium and hafnium have high atomic masses $[m_{\mathrm{at}}(\mathrm{Y}) = 89$ u and $m_{\mathrm{at}}(\mathrm{Hf}) = 178$ u], fewer atoms are required to form nanoparticles of high mass. This will later allow forming particles of 10^8 Da without the cluster size exceeding the period of a UV standing light wave [22].

The overall layout of the experiment is shown in Fig. 1. It utilizes a DC magnetron sputter source, a UV photodepletion stage as a probe for future matter-wave gratings, and a high-mass quadrupole mass filter where neutral clusters can

be ionized and counted after secondary electron multiplication via a conversion dynode.

The first ultraviolet laser beam is used to deplete the particle beam in mass-selective measurements of cluster beam velocity and ionization cross sections. For that purpose it can be mechanically chopped to imprint a time-modulated depletion signal. The second laser beam is positioned within the ion region of the quadrupole mass detector stage to complement the electron impact ionization. This allows us to compare electron impact with UV photoionization for both materials in all cluster number states and for all velocities. The two laser beams are separated by 0.93 m. This gives the neutral clusters sufficient travel time to obtain their velocity distributions via time-of-flight measurements.

Two UV laser beams are generated by second harmonic generation (SHG) of which each is pumped with 4 W of green laser light (532 nm, Coherent Verdi V18, 10 MHz linewidth) in two frequency doubling cavities (Newport Wavetrain 2). The intensity of the beams is adjusted by polarization optics. We obtain routinely about 1 W of 266 nm radiation in each of the two elliptical Gaussian beams. The doubling cavities are purged with purified air and the emitted UV intensity is stable over ~10 h with an average power loss of 3% per hour. This can be compensated by a slight cavity re-alignment or a shift of the doubling crystal.

The mass spectrometer is a custom-made adaptation of a quadrupole mass filter (Oxford Applied Research) which we have augmented with an electron impact ionization stage and a secondary electron multiplier with conversion dynode (CMS Extrel). Even though electron impact ionization can be applied to a large variety of molecules and nanoparticles, the available electron flux is usually space-charge limited and can be easily outperformed by the photon flux of Watt-level

ultraviolet light. The UV absorption properties also determine the feasibility of future ionization gratings for metal cluster diffraction and interference [25,26].

Efficient secondary electron multiplication on the dynode and subsequent ion detection with a quantum yield close to one requires ion velocities of $v_{ion} > 20\,000$ m/s, i.e., energies $E > 100$ keV for clusters of $m > 100$ kDa [28]. Our dynode voltage is currently limited to 10 kV. All count rates shown below are therefore lower bounds to values that can be improved by adding a high-voltage detector [29]. The absolute cross-section measurements below are unaffected by the absolute quantum yield as they can be derived from normalized count rates.

III. RESULTS

While the semiclassical Drude-Lorentz model can predict optical absorption cross sections and optical polarizabilities, ionization efficiencies depend on the details of the electronic states. It is therefore more practical to measure these properties. Likewise, cluster mass and velocity distributions are kinematic properties that are best determined experimentally.

A. Cluster formation and detection

Cluster aggregation is expected to follow a log-normal distribution in the number N of atoms per cluster [30]. However, the detected distribution can deviate from this law because the cross section for both electron impact and single-photon ionization increase while the quadrupole transmission and secondary electron conversion decrease with cluster mass.

The mean number of photons absorbed by a cluster of cross section σ_{abs} is determined by the laser power P in an elliptical Gaussian beam waist $w_x \times w_y$, the photon wavelength λ, and the interaction time which is determined by the molecular forward velocity v_x. Integrating over the laser beam profile in forward direction yields

$$n_{abs} = \int_{-\infty}^{\infty} \frac{2P\sigma_{abs}\lambda}{\pi\, w_x w_y v_x hc} e^{-2x^2/w_x^2} dx = \sqrt{\frac{2}{\pi}} \frac{P\sigma_{abs}\lambda}{w_y v_x hc}. \quad (1)$$

Single-photon ionization requires the photon to exceed the ionization energy which approaches the work function of the bulk W with increasing cluster radius R:

$$E_{ion} = W + \alpha \frac{e^2}{4\pi\varepsilon_0 R} \quad (2)$$

where $\alpha \simeq 3/8$ [31] and the radius is $R = (3m/4\pi\rho)^{1/3}$. In Fig. 2 we have used this equation to compute the mass dependence work function of Y and Hf clusters. We find for $m = 100$ kDa the energies $E_{ion}(Y) = 3.36$ eV and $E_{ion}(Hf) = 4.28$ eV. However, 0.5–1 eV higher photon energies are required to saturate the ionization efficiency and to maximize the transition to the resulting cluster ion state.

Figure 3 compares the mass spectrum of yttrium under electron impact ionization and photoionization with the results of hafnium under identical ionization parameters. The UV laser beam of the detection stage was retroreflected using a flat mirror to enhance the intensity to an average of 50 W/cm². We detect metal clusters in a mass range of 60–600 kDa with counts of several 100 kcps in a continuous
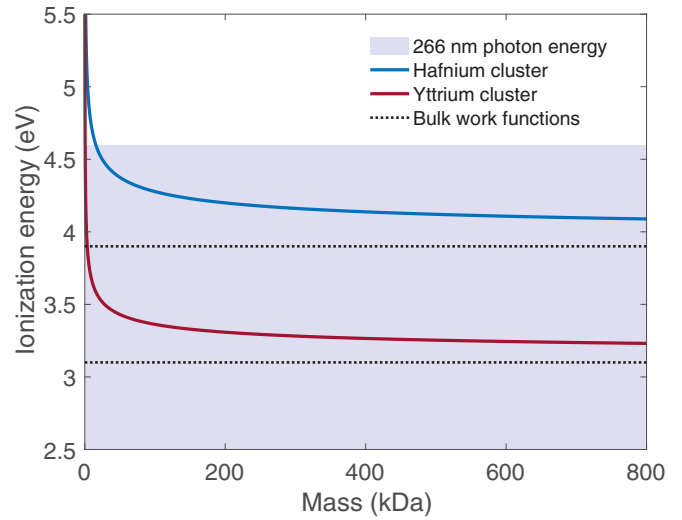

FIG. 2. Ionization energies for yttrium and hafnium clusters as a function of mass using Eq. (2). The dotted line represents the bulk work functions of the metals and the shaded purple area the single photon energy of a 266 nm UV laser light. While even small yttrium clusters can be ionized with 266 nm, the ionization energy of hafnium clusters is sufficiently low from about 100 kDa and above.

cluster beam that is collimated to 3×3 mm² in 2 m distance behind the source.

While the low single photon energy of the photoionization in comparison to the ionization energies of the clusters allows us to assume singly charged cluster ions as the only present charge state, the higher energies of electron-impact ionization ($\sim$60 eV) can in principle also lead to multiple charge states. However, we could not observe a strong presence of multiply
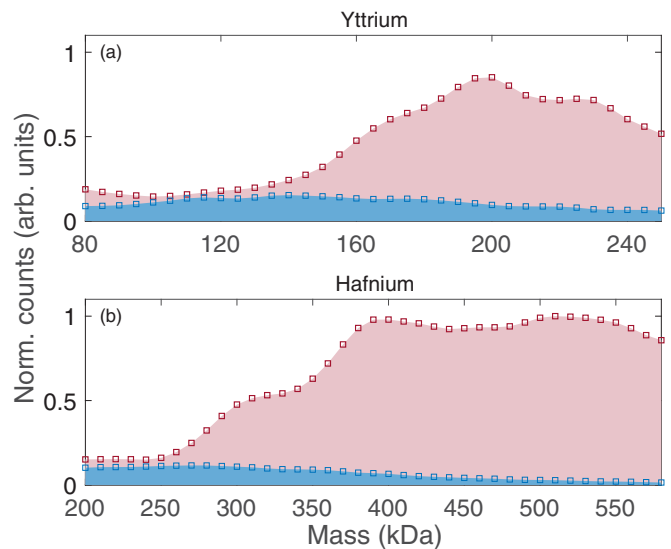

FIG. 3. Detected mass distribution in the range of 80–600 kDa for (a) yttrium and (b) hafnium upon electron impact ionization (blue area) and 266 nm photoionization (pink area). The detected solid angle is $d\Omega \simeq 10^{-6}$ sr. UV photoionization improved the count rates manifold compared to electron impact ionization. The advantage grows with the cluster mass as this increases the absorption cross section and lowers the ionization energy. The mass resolution is 7%.
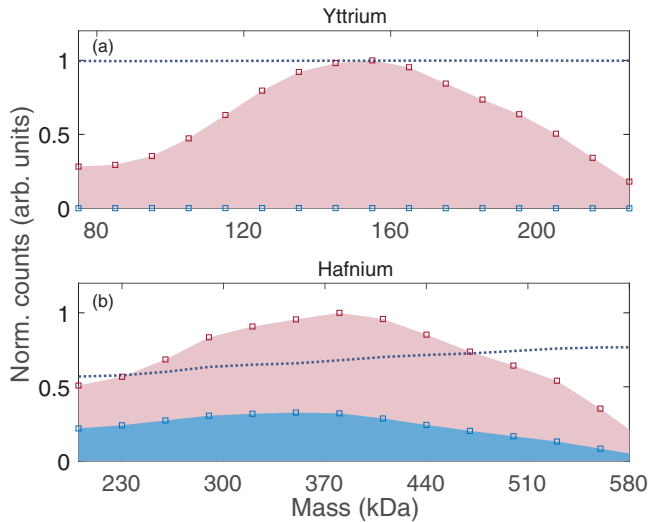
FIG. 4. Detected mass distributions with (blue area) and without (pink area) the depletion laser for (a) yttrium and (b) hafnium clusters. The dotted line represents the depletion efficiency at each mass. The laser intensity for the shown depleted mass spectra was $I_0 = 16$ W cm^{-2} and $I_0 = 12$ W cm^{-2}, respectively. Yttrium clusters saturate at lower laser power than hafnium clusters, which can be attributed to their higher ionization cross sections. For lower laser powers the yttrium clusters show a mass dependent depletion behavior similar to that of hafnium, shown in (b). The mass resolution was 7%.
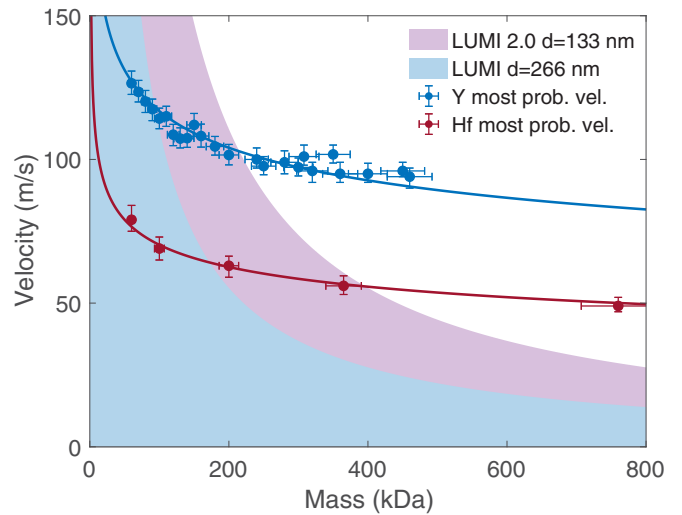

FIG. 5. Most probable velocities of mass-selected yttrium (orange) and hafnium (blue) clusters. The velocity distributions were obtained via a time-of-flight measurement of the neutral cluster beam by chopping the beam into packets with the depletion laser. The lines are fits to a power law $v(m) = am^{-1/6}$ to provide a guide to the eye. The purple area represents the compatible de Broglie wavelengths for the current interferometer setup (LUMI) [12] and the pink area for the next generation matter-wave interferometer using three UV 266 nm laser gratings. The uncertainties on the x axis are given by the 7% mass resolution of the quadrupole mass filter. The error bars on the y axis show the systematic errors of the time-of-flight measurements.

charged cluster ions in our recorded spectra. For all other measurements we have used the photoionization scheme for the detection, where we can safely assume the detected clusters to be singly charged ions.

The count rates were substantially higher for photoionization than for electron impact. Depending on the cluster material and mass, the relative enhancement can be up to 40-fold. While yttrium shows increased counts already for $m < 100$ kDa, the benefits of photoionization emerged for $m > 200$ kDa in the case of hafnium. The higher ionization efficiency of yttrium can be attributed to its lower ionization energies. However, under similar aggregation conditions hafnium emits a higher flux of clusters beyond $m > 200$ kDa. Combining the advantages of each material allows us to span our measurements over the entire mass range.

B. Beam depletion and velocity distributions

In order to realize depletion gratings, we have to ensure that the nanoparticles deplete efficiently with available UV laser intensities. In Fig. 4 we show the depletion of the mass spectra for (a) yttrium and (b) hafnium for laser intensities of $I_0 = 16$ W cm^{-2} and $I_0 = 12$ W cm^{-2}, respectively, in a beam waist of $w_x \times w_y = 1.4 \times 1.9$ mm^2. The cluster beam was transmitted through a pinhole of $d = 300$ μm to control the overlap with the laser beam. While the depletion of the whole detected mass range of yttrium clusters already saturates at moderate laser power, higher intensities are needed for the hafnium clusters.

The same depletion laser was then also modulated by a mechanical chopper to realize an optical chopper for the cluster

beam. In combination with an arrival time measurement in the quadrupole detector, this allows us to determine a velocity distribution of the mass-selected neutral cluster beam.

The cluster velocities depend on the aggregation gas and plasma settings [32,33]. For the given measurements the argon aggregation pressure was approximately 1 mbar and the plasma power ranged from 50–150 W. The aggregation length varied between 10–150 mm to control the cluster size distribution. The wall of the aggregation tube is water cooled to room temperature. The aggregation chamber is separated from the depletion chamber by a differential pumping stage with an entrance pinhole of 4 mm diameter and closed by a 3 mm skimmer, which keeps the photodepletion region at 10^{-5} mbar.

We have measured beam velocities in the range of 100–140 m/s for yttrium and 50–120 m/s for hafnium with masses ranging from 80–500 kDa and 90–800 kDa, respectively. The measured velocities are shown in Fig. 5 as a function of mass, together with compatible de Broglie wavelenghts for current and future matter-wave interferometers. The velocity slip increases with increasing cluster size. For both materials the full width at half maximum (FWHM) of the velocity distribution remained $\Delta v/v < 10\%$. Velocity measurements of copper nanoparticles from a magnetron aggregation source found a simple power-law mass dependence of the cluster velocities [34]. We therefore fit $v(m) = am^{-b}$ with a as a free parameter to the velocity data. Where m is the cluster mass in kDa. We found that $b = 1/6$ achieves good fit results for both data curves and resulting values of
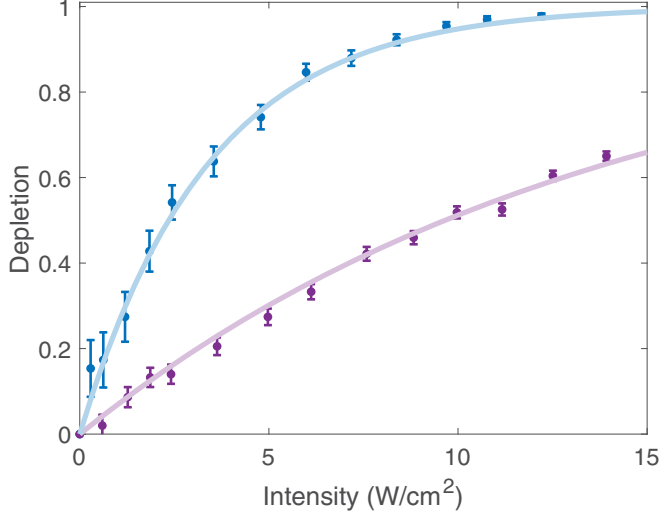
FIG. 6. Depletion efficiency of yttrium and hafnium clusters as a function of depletion laser power. Here we show the saturation curve of yttrium clusters (blue) at a mass of 100 kDa and hafnium clusters (purple) at 350 kDa. Similar depletion curves were measured for varying cluster sizes in a mass range of 80–600 kDa. The UV laser power was scanned from 0–510 mW for yttrium and 0–582 mW for hafnium with an absolute uncertainty of ± 5 mW. The error bars on the y axis show 1σ uncertainties and have been estimated using Poissonian statistics on the count rates. The solid lines are the fits of Eq. (3) to the data points with the photoionization cross section σ_{PI} as the only free parameter.

$a_Y = 252$ kDa$^{1/6}$ ms^{-1} and $a_{Hf} = 151$ kDa$^{1/6}$ ms^{-1}. The fits are meant to be viewed as a guide to the eye.

C. Photoionization cross sections

Knowing the laser beam profile and intensity as well as the cluster size and velocity, we can determine the photoionization cross sections σ_{PI} from a fit to the saturation curve (Fig. 6) for yttrium and hafnium, as shown in Fig. 7

$$S(P) = 1 - \exp\left(-\sqrt{\frac{2}{\pi}} \frac{\sigma_{PI} P_L \lambda_L}{hc v_x w_y} \int_{-y_0}^{y_0} \frac{1}{2y_0} e^{\frac{-2y^2}{w_y^2}} dy\right), \quad (3)$$

with $2y_0$ being the effective overlap between the laser beam and the molecular beam, which in our case is defined by the diameter of the pinhole $2y_0 = 300 \, \mu$m. The measured depletion efficiency can be used to obtain the mass-dependent photoionization cross section of the clusters by fitting the data to the saturation curve.

For each depletion scan we have measured the mass-dependent cluster velocities, the laser beam waist, and power. With this we have derived absolute values for the photoionization cross section σ_{PI} at 266 nm for yttrium and hafnium in a mass range of 60–300 kDa and 100–600 kDa, respectively. The cross sections are about an order of magnitude larger for yttrium ($\sim 10^{-14}$ cm^2) than for hafnium ($\sim 10^{-15}$ cm^2).

The Drude-Lorentz model predicts a linear increase of the absorption cross section with cluster mass. The measured photoionization cross sections are a product of the absorption cross section and the ionization probability. For massive clusters the two cross sections should be the same [35]. We have
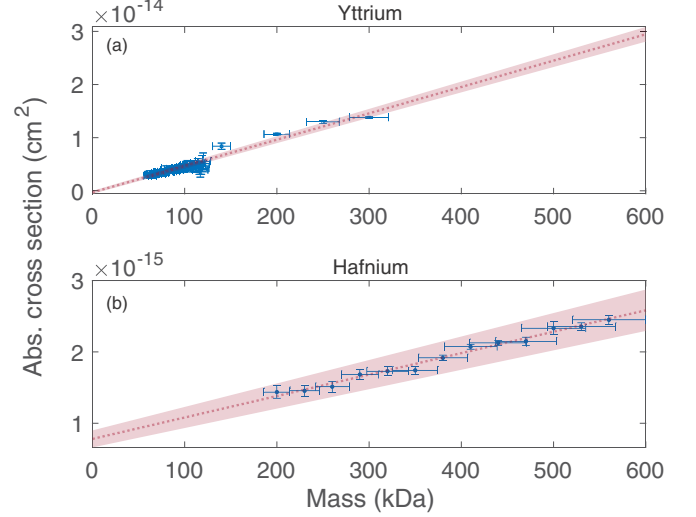

FIG. 7. Photoionization cross section at 266 nm for mass-selected yttrium (a) and hafnium clusters (b). The cross sections were obtained by fitting the saturation curves to the mass-dependent depletion at different laser powers. To first order we can take the results of the linear fit (dotted line) to give absolute values of σ_{PI} as a function of mass for the measured mass range. The shaded area shows the 95% confidence bounds of the linear fit. The error bars on the y axis represent the 95% confidence bounds of the individual fits as shown in Fig. 6. The uncertainties on the x axis are given by the 7% mass resolution of the quadrupole mass filter.

applied linear fits with an offset to our mass-dependent cross sections. The fit can be used to extrapolate the photoionization cross section to clusters of higher masses. For yttrium we obtain

$$\sigma_{PI,Y} = (5 \times 10^{-17} m/\text{kDa} - 3 \times 10^{-16}) \, \text{cm}^2$$

and for hafnium the values are

$$\sigma_{PI,Hf} = (3 \times 10^{-18} m/\text{kDa} + 8 \times 10^{-16}) \, \text{cm}^2.$$

We can compare these measurements to the semiclassical model for the absorption cross section of a hafnium cluster of $m = 500$ kDa irradiated by light with a wavelength of $\lambda = 266$ nm:

$$\sigma_{abs,Hf} = \frac{6\pi m}{\lambda \rho} \text{Im} \frac{\varepsilon - 1}{\varepsilon + 2} \simeq 2.3 \times 10^{-15} \, \text{cm}^2, \quad (4)$$

where

$$\varepsilon(\omega) = 1 - \frac{\omega_p^2}{\omega(\omega + i\gamma_p)} \quad (5)$$

is given by the plasma frequency $\omega_p = \sqrt{n_e e^2/m_e \varepsilon_0}$, with the electron density $n_e(\text{Hf}) = 1.5 \times 10^{29}$ m^{-3} and electron mass m_e, the DC resistivity $\rho_{DC} = 3.4 \times 10^{-7}$ Ωm and thus the plasma oscillation damping rate [22]

$$\gamma_p = \omega_p^2 \varepsilon_0 \rho_{DC} + \frac{4\hbar}{3 m_e R}(3\pi^2 n_e)^{1/3} = 3.47 \times 10^{15} \, \text{s}^{-1}. \quad (6)$$

The predicted theory value agrees well with the measured photoionization cross section of hafnium at $m = 500$ kDa with $\sigma_{PI} = 2.3 \times 10^{-15}$ cm^2. However, the linear fits require an offset and also the slope differs from the theoretical prediction. This can be attributed to the ionization energies, which could

still be too high to ensure sufficient single-photon ionization, especially for smaller hafnium clusters.

IV. CONCLUSION AND PROSPECTS FOR MATTER-WAVE INTERFEROMETRY

The goal of this study was to identify and characterize metal clusters that fulfill the requirements for a next generation matter-wave interferometer. We have picked yttrium and hafnium due to their magnetic, optical, and cluster forming properties. Using a DC magnetron aggregation source we are able to produce neutral cluster beams in a range of 60–800 kDa with detection rates of up to a million counts per second, even at moderate post-acceleration for the most massive ions. Given the brilliance of 10^{11} sr^{-1} s^{-1} clusters of the magnetron source and the geometry of the existing long-baseline universal matter-wave interferometer [12] but with upgraded UV gratings, we expect count rates in the order of 1000 cts/s during interference scans.

The mean cluster velocities range from 50–140 m/s with a narrow FWHM <10%. The resulting de Broglie wavelenghts of about $\lambda_{dB} \simeq 20$ fm are compatible with the layout of a next-generation Talbot-Lau interferometer with three gratings of period $d = 133$ nm, as shown in Fig. 5. We have shown that the power, wavelength, and stability of our UV laser system suffices to efficiently ionize and deplete the metal cluster beam. Photoionization can be two orders of magnitude more efficient than electron impact in the continuous cluster beam and it will allow the realization of standing light wave gratings.

The high photoionization cross section at 266 nm makes yttrium a perfect first candidate for exploring cluster matter-wave interferometry for clusters from 30 to 200 kDa. Above 200 kDa hafnium appears more favorable, since it aggregates preferably to more massive clusters. Despite its lower ionization efficiency compared to yttrium, the heavier clusters will ionize and deplete efficiently. Hafnium promises to push the limits of macroscopcic matter-wave interference to almost half a million atomic mass units using an all-optical interferometer.

The same source and detection mechanism are also expected to facilitate future upgrades to even higher masses. Modern laser technology will soon allow creating gratings with several 100 mW of 225 nm light. The higher photon energy would enable experiments with an even larger variety of metals and semiconductors. Alternative metal cluster interferometry schemes could extend the mass scale to >10^7 Da [22]. The laser power requirements in such a regime would be relaxed, since ionization cross sections increase with increasing mass.

---

[1] A. Bassi, K. Lochan, S. Satin, T. P. Singh, and H. Ulbricht, Models of wave-function collapse, underlying theories, and experimental tests, Rev. Mod. Phys. **85**, 471 (2013).

[2] L. Diosi, Gravitation and quantum-mechanical localization of macro-objects, Phys. Lett. A **105**, 199 (1984).

[3] R. Penrose, On gravity's role in quantum state reduction, Gen. Relativ. Gravit. **28**, 581 (1996).

[4] C. J. Riedel and I. Yavin, Decoherence as a way to measure extremely soft collisions with dark matter, Phys. Rev. D **96**, 023007 (2017).

[5] P. M. Bonifacio, C. H. T. Wang, J. T. Mendona, and R. Bingham, Dephasing of a non-relativistic quantum particle due to a conformally fluctuating spacetime, Classical Quantum Gravity **26**, 145013 (2009).

[6] I. Pikovski, M. Zych, F. Costa, and C. Brukner, Universal decoherence due to gravitational time dilation, Nat. Phys. **11**, 668 (2015).

[7] J. Rodewald, N. Dörre, A. Grimaldi, P. Geyer, L. Felix, M. Mayor, A. Shayeghi, and M. Arndt, Isotope-selective high-order interferometry with large organic molecules in free fall, New J. Phys. **20**, 033016 (2018).

[8] A. D. O'Connell, M. Hofheinz, M. Ansmann, R. C. Bialczak, M. Lenander, E. Lucero, M. Neeley, D. Sank, H. Wang, M. Weides, J. Wenner, J. M. Martinis, and A. N. Cleland, Quantum ground state and single-phonon control of a mechanical resonator, Nature (London) **464**, 697 (2010).

[9] U. Delic, M. Reisenbauer, K. Dare, D. Grass, V. Vuleti, N. Kiesel, and M. Aspelmeyer, Cooling of a levitated nanoparticle to the motional quantum ground state, Science **367**, 892 (2020).

[10] M. Zawisky, M. Baron, R. Loidl, and H. Rauch, Testing the worlds largest monolithic perfect crystal neutron interferometer, Nucl. Instrum. Methods Phys. Res. Sect. A **481**, 406 (2002).

[11] T. Kovachy, P. Asenbaum, C. Overstreet, C. A. Donnelly, S. M. Dickerson, A. Sugarbaker, J. M. Hogan, and M. A. Kasevich, Quantum superposition at the half-metre scale, Nature (London) **528**, 530 (2015).

[12] Y. Y. Fein, P. Geyer, P. Zwick, F. Kiaka, S. Pedalino, M. Mayor, S. Gerlich, and M. Arndt, Quantum superposition of molecules beyond 25 kDa, Nat. Phys. **15**, 1242 (2019).

[13] A. Shayeghi, P. Rieser, G. Richter, U. Sezer, J. H. Rodewald, P. Geyer, T. J. Martinez, and M. Arndt, Matter-wave interference of a native polypeptide, Nat. Commun. **11**, 1447 (2020).

[14] U. Sezer, P. Schmid, L. Felix, M. Mayor, and M. Arndt, Stability of high-mass molecular libraries: The role of the oligoporphyrin core, J. Mass Spectrom. **50**, 235 (2015).

[15] A. Gallego, U. Sezer, M. Arndt, and M. Mayor, Long-pulse laser launch and ionization of tailored large neutral silver nanoparticles with atomic mass assignment, Nanoscale **9**, 9175 (2017).

[16] K. Tanaka, H. Waki, Y. Ido, S. Akita, Y. Yoshida, and T. Yoshida, Protein and polymer analyses up to *m/z* 100 000

by laser ionization time-of-flight mass spectrometry, Rapid Commun. Mass Spectrom. **2**, 151 (1988).

[17] M. Karas and F. Hillenkamp, Laser desorption ionization of proteins with molecular mass exceeding 10,000 daltons, Anal. Chem. **60**, 2299 (1988).

[18] U. Sezer, L. Wörner, J. Horak, L. Felix, J. Tüxen, C. Götz, A. Vaziri, M. Mayor, and M. Arndt, Laser-induced acoustic desorption of natural and functionalized biochromophores, Anal. Chem. **87**, 5614 (2015).

[19] P. Asenbaum, S. Kuhn, S. Nimmrichter, U. Sezer, and M. Arndt, Cavity cooling of free silicon nanoparticles in high-vacuum, Nat. Commun. **4**, 2743 (2013).

[20] W. P. Peng, S. W. Chou, and A. A. Patil, Measuring masses of large biomolecules and bioparticles using mass spectrometric techniques, Analyst **139**, 3507 (2014).

[21] D. S. Bykov, P. Mestres, L. Dania, L. Schmöger, and T. E. Northup, Direct loading of nanoparticles under high vacuum into a Paul trap for levitodynamical experiments, Appl. Phys. Lett. **115**, 034101 (2019).

[22] F. Kiałka, Y. Y. Fein, S. Pedalino, S. Gerlich, and M. Arndt, A roadmap for universal high-mass matter-wave interferometry, AVS Quantum Sci. **4**, 020502 (2022).

[23] N. Dörre, J. Rodewald, P. Geyer, B. von Issendorff, P. Haslinger, and M. Arndt, Photofragmentation Beam Splitters for Matter-Wave Interferometry, Phys. Rev. Lett. **113**, 233001 (2014).

[24] U. Sezer, P. Geyer, M. Kriegleder, M. Debiossac, A. Shayeghi, M. Arndt, F. L, and M. Mayor, Selective photodissociation of tailored molecular tags as a tool for quantum optics, Beilstein J. Nanotechnol. **8**, 325 (2017).

[25] E. Reiger, L. Hackermüller, M. Berninger, and M. Arndt, Exploration of gold nanoparticle beams for matter wave interferometry, Opt. Commun. **264**, 326 (2006).

[26] P. Haslinger, N. Dörre, P. Geyer, J. Rodewald, S. Nimmrichter, and M. Arndt, A universal matter-wave interferometer with optical ionization gratings in the time domain, Nat. Phys. **9**, 144 (2013).

[27] H. Haberland, M. Karrais, and M. Mall, A new type of cluster and cluster ion source, Z. Phys. D: At. Mol. Clusters **20**, 413 (1991).

[28] R. J. Beuhler and L. Friedman, Threshold studies of secondary electron emission induced by macro-ion impact on solid surfaces, Nucl. Instrum. Methods Phys. Res. Sect. A **170**, 309 (1980).

[29] N. R. Daly, Scintillation type mass spectrometer ion detector, Rev. Sci. Instrum. **31**, 264 (1960).

[30] I. Pöcsik, Lognormal distribution as the natural statistics of cluster systems, Z. Phys. D: At. Mol. Clusters **20**, 395 (1991).

[31] M. Seidl, K.-H. Meiwes-Broer, and M. Brack, Finite-size effects in ionization potentials and electron affinities of metal clusters, J. Chem. Phys. **95**, 1295 (1991).

[32] B. M. Smirnov, I. Shyjumon, and R. Hippler, Flow of nanosize cluster-containing plasma in a magnetron discharge, Phys. Rev. E **75**, 066402 (2007).

[33] M. Ganeva, A. V. Pipa, B. M. Smirnov, P. V. Kashtanov, and R. Hippler, Velocity distribution of mass-selected nano-size cluster ions, Plasma Sources Sci. Technol. **22**, 045011 (2013).

[34] P. Solař, K. Škorvánková, A. Kuzminova, J. Kousal, and O. Kylián, Measurement of velocities of copper nanoparticles exiting a gas aggregation source, Vacuum **202**, 111114 (2022).

[35] M. Koskinen and M. Manninen, Photoionization of metal clusters, Phys. Rev. B **54**, 14796 (1996).